


Multi-Response Au-Nanohybrid Composite Triggered NIR-Light for Effective Anti-Tumor Therapy in Animal Model

Ling-zhijie Kong^{1,*}, Dong Zhou^{2,*}, Guoyan Mo^{3,*}, Mingyue Shu³, Wenyan Yu¹, Hao Cheng¹, Kaichun Li¹ 

¹Department of Oncology, Shanghai Fourth People's Hospital, Tongji University School of Medicine, Shanghai, 200434, People's Republic of China;

²The State Key Laboratory of Bioreactor Engineering and Key Laboratory for Ultrafine Materials of Ministry of Education, East China University of Science and Technology, Shanghai, 200237, People's Republic of China; ³China Key Laboratory of TCM Resource and Prescription, Ministry of Education, Hubei University of Chinese Medicine, Wuhan, 430065, People's Republic of China

*These authors contributed equally to this work

Correspondence: Kaichun Li, Email likaichun@tongji.edu.cn

Introduction: The therapeutic efficacy of nanomedicine in oncology is predicated on its capacity to enhance drug uptake by cells and control drug release. While targeted nanomedicines are highly regarded for their potential, they are not spared from issues of colloidal instability and uncontrolled drug release.

Methods: The hybrid system (Au@SiO₂-HA-DOX) was designed to enhance colloidal stability and facilitate controlled drug delivery by coating gold nanorods with silica shells and hyaluronic acid (HA) for tumor targeting. The nanoparticles were characterized for morphology, size, zeta potential, and photothermal properties. The loading efficiency of doxorubicin (DOX) and its release behavior in response to pH, reactive oxygen species (ROS), and NIR stimulation were evaluated.

Results: Under NIR irradiation, the nanoparticles exhibited excellent photothermal stability and sustained temperature elevation. In vitro studies demonstrated that the nanoparticles possessed good biocompatibility (cell viability exceeding 90%) and colloidal stability (7 days). The loading efficiency of DOX was enhanced to 65.9%, with sustained release characteristics. Furthermore, Au@SiO₂-HA-DOX exhibited selective targeting and stronger cytotoxicity towards cancer cells. The cellular uptake efficiency was 1.7 times higher than that of the Free DOX at 24 h, with an IC₅₀ value of 1.36 μ M, compared to 2.01 μ M for Free DOX. In vivo experiments in a mouse breast cancer model revealed significant tumor growth inhibited with NIR-assisted therapy, while maintaining stable body weight and preserving good biocompatibility.

Conclusion: This nanohybrid system represents a promising strategy for improving the efficacy of chemotherapy and reducing toxicity in cancer treatment. It enhances drug enrichment and release in tumor tissues while minimizing the impact on normal tissues.

Keywords: gold nanorods, high colloidal stability, pH/ROS-responsive, tumor microenvironment, tumor-targeted therapy

Introduction

Cancer is characterized by the uncontrolled proliferation of cells that evade immune surveillance and continues to poses a significant challenge in clinical oncology.¹ Traditional therapies, including surgery,² radiotherapy,³ and chemotherapy,⁴ are often limited by their systemic toxicity and associated adverse effects. The advancement of nanotechnology has facilitated a paradigm shift in tumor treatment, with nanomaterials presenting significant potential for targeted drug delivery.^{5,6} These nanoscale carriers can preferentially accumulate in tumor tissues, thereby enhancing therapeutic efficacy while minimizing off-target toxicity.⁷ However, the clinical translation of nanomedicine remains limited due to suboptimal tumor penetration and the relatively low proportion of nanoparticles (NPs) that reach the tumor site via the enhanced permeability and retention (EPR) effect.^{8,9} Moreover, the elevated interstitial pressure in the tumor micro-environment further restricts the diffusion and distribution of therapeutic agents, ultimately compromising the efficacy of

nanomedicines.¹⁰ Consequently, the design and development of nanomedicines with improved tumor targeting and penetration capabilities is crucial for the continued advancement of cancer nanotherapeutics.¹¹

Near-infrared (NIR) light-triggered systems have emerged as a promising strategy for enhancing the therapeutic efficacy of nanomaterials in cancer treatment.¹² These systems utilize NIR light as an external stimulus to achieve specific functions through light absorption and conversion.¹³ The core of this approach lies in converting the energy of NIR light into other forms of energy, such as heat, to facilitate drug release, photothermal therapy, and photodynamic therapy.¹⁴ The integration of photothermal therapy with nanomaterials has emerged as a cutting-edge strategy in the management of solid tumors.¹⁵ This approach leverages local near-infrared (NIR) light irradiation to transiently increase the permeability of tumor cells,¹⁶ facilitating the penetration of nanomaterials and inducing localized hyperthermia.¹⁷ The latter can lead to protein denaturation,¹⁸ cell membrane disruption, and eventually tumor cell death.¹⁹ However, a delicate balance must be maintained; excessive temperatures can result in collateral damage to healthy tissues and uncontrolled drug release.²⁰ Therefore, achieving controlled drug penetration within tumors through moderate NIR stimulation is a key factor of this therapeutic modality.²¹ A wide array of photothermal agents has been explored for tumor ablation,²² including organic small molecules and inorganic materials such as graphene oxide,²³ black phosphorus nanosheets,²⁴ sulfides,²⁵ and metal nanoparticles.²⁶ Among these, gold nanorods (GNRs) are particularly notable due to their tunable aspect ratios and high photothermal conversion efficiency,²⁷ making them a widely used choice in cancer therapy.²⁸ GNRs possess a large specific surface area, enabling functionalization with various moieties to create multifunctional nanomedicines. For instance,²⁸ the stability of GNRs can be enhanced by coating them with a silica shell, which also minimizes their cytotoxicity.²⁹ However, the lack of tumor-specific targeting remains a critical challenge that needs to be addressed.

CD44 is a transmembrane protein overexpressed in cancer cells, and it is closely associated with tumorigenesis and metastatic potential.³⁰ Hyaluronic acid (HA), known for its high affinity to CD44 receptors on cancer cells, has emerged as a promising ligand for targeted drug delivery to tumor tissues.³¹ However, upon reaching the tumor microenvironment, characterized by elevated reactive oxygen species (ROS)³² and acidic pH,³³ conventional nanomedicines often face challenges in achieving sustained and effective drug release.³⁴ This limitation has spurred the development of nanocarriers that are responsive to the tumor-specific microenvironment, facilitating controlled and sustained drug release.³⁵ Alternatively, nanomedicines targeting tumor tissues, including GNRs modified with HA and folic acid, have been harnessed to address the above-mentioned limitation.³⁶ Despite their potential, these nanomedicines often exhibit limited control over drug release dynamics, resulting in suboptimal therapeutic outcomes. ROS plays a pertinent role in tumorigenesis, metastasis, and drug resistance, presenting an opportunity for modulating the tumor microenvironment.³⁷ Strategies that target ROS to reverse the tumor microenvironment and inhibit tumor recurrence and metastasis are of significant interest.³⁸ Nanomedicines with unique structures capable of responding to ROS stimuli for drug release have been developed via incorporating dynamic covalent bonds such as disulfides, diselenides, and boronate esters.³⁹ Notably, boronate esters are dynamic covalent bonds that can scavenge ROS in a low ROS environment, facilitating drug release.⁴⁰ Therefore, the development of targetable nanocarriers with controllable drug release based on boronate esters represents a pivotal strategy in cancer therapy.

Herein, we introduce a novel GNRs-based hybrid system that is triggered by NIR light, designed to address the challenges of colloidal stability and controlled drug delivery within the tumor microenvironment. This system is capable of not only selectively targeting tumor tissues but also delivering therapeutic agents in a sustained and tumor-specific manner. The GNRs are well-known for their excellent photothermal properties, which serve as the core of the hybrid system. To enhance their stability, we have deposited silica shells on their surface, which also creates a porous structure that significantly increases drug loading capacity. Subsequently, DOX is efficiently encapsulated within NPs, leveraging the hydroxyl groups of boric acid and HA. This strategic design endows the NPs with the dual capability of tumor tissue targeting and enhanced responsiveness. Our findings demonstrate that these NPs can respond to NIR, pH, and ROS stimuli, thereby controlling and sustaining drug release. Moreover, they selectively target tumor cells and exhibit enhanced cell uptake under NIR light stimulation conditions. The dynamic cross-linking within this nanohybrid system positions it as a promising candidate for a new class of nanocarriers in targeted tumor therapy.

Materials and Methods

Cetyltrimethylammonium bromide (CTAB), 1-(3-(dimethylamino)-propyl)-3-ethylcarbodiimide hydrochloride (EDC·HCl), N-hydroxysuccinimide (NHS) and sodium borohydride (NaBH_4) were procured from Sinopharm Chemical Reagent Co., Ltd. (Shanghai, China). Gold(III) chloride trihydrate ($\text{HAuCl}_4 \cdot 3\text{H}_2\text{O}$), tetraethyl orthosilicate (TEOS), carboxyphenylboronic acid (CPBA) and 3-aminopropyltriethoxysilane (APTES) were sourced from Aladdin Chemical Reagent Co., Ltd. (Shanghai, China). Hyaluronic acid (HA) (MW = 50 kDa) was obtained from Freda Biochem Co. Ltd. (Shandong, China). Doxorubicin (DOX) was purchased from Dalian Meilun Biotechnology Co., Ltd. (Dalian, China). L929 cells and MCF-7 cells were purchased from the Cell Bank of the Type Culture Collection of the Chinese Academy of Sciences (Shanghai, China).

Synthesis of Gold Nanorods

GNRs were synthesized via the seed growth method following a previous report.⁴¹ Briefly, 0.25 mL of a 0.01 M $\text{HAuCl}_4 \cdot 3\text{H}_2\text{O}$ solution was added into 9.75 mL of a 0.1 M CTAB solution and mixed thoroughly. Subsequently, 0.6 mL of an ice-cold 0.01 M NaBH_4 solution was added, and the mixture was stirred vigorously for 10 min. The resulting solution was maintained at 27 °C for 1.5 h to obtain the seed solution. For the growth solution, 0.5 mL of a 0.01 M $\text{HAuCl}_4 \cdot 3\text{H}_2\text{O}$ solution was mixed with 8 mL of a 0.1 M CTAB solution, followed by the sequential addition of 0.1 mL of a 0.01 M AgNO_3 solution, 0.2 mL of a 1.0 M HCl solution, 80 μL of a 0.1 M ascorbic acid solution, and 2 mL of the seed solution. The resulting mixture was gently inverted and allowed to stand at 27 °C for 20 h. The GNRs were collected by centrifugation at $10,000 \times g$ for 20 min.

Synthesis of Gold Nanohybrid Composites

The GNRs were re-dispersed in a CTAB solution, and the pH was adjusted to 10.5 by adding a 0.1 M NaOH solution. A mixture of TEOS/MeOH (20% v/v) was added in 300 μL aliquots, three times at 30-min intervals, with continuous stirring for 6 h to obtain Au@SiO_2 nanoparticles. To remove CTAB, the nanoparticles were dispersed in a mixture of 10 mL of ethanol and HCl (1% v/v) and refluxed at 80 °C for 6 h. The resulting particles were washed three times. Subsequently, the nanoparticles were re-dispersed in 100 mL of anhydrous ethanol, followed by the addition of 1 mL of an APTES, and the mixture was stirred at 80 °C for 24 h to functionalize the surface with amino groups. The amino-modified Au@SiO_2 nanoparticles were collected after 10,000 rpm and centrifugal washing with anhydrous ethanol and purified water for three times, respectively.

To conjugate CPBA, a solution containing 0.3 g CPBA, 0.2 g NHS, and 0.4 g EDC in 10 mL of DMSO was stirred for 30 min at room temperature. Then, 20 mL of a DMSO solution containing Au@SiO_2 nanoparticles was added and stirred continuously for 24 h to obtain Au@SiO_2 -CPBA nanoparticles. The purified nanoparticles were subsequently mixed with an aqueous HA solution and stirred for 3 h to obtain Au@SiO_2 -HA nanoparticles.

Characterization of Different Nanoparticles

The morphology of Au-NRs and Au@SiO_2 -HA was characterized using transmission electron microscopy (JEM-2100P, Japan). The microstructure of Au-NRs and Au@SiO_2 -HA was examined using Fourier-transform infrared spectroscopy (FTIR, Nicolet iS20, USA). The light absorption properties of nanoparticles were measured using ultraviolet-visible spectrophotometry (UV-3600i Plus, Japan). The hydrodynamic diameter and surface charge of the different nanoparticles were examined using dynamic light scattering (DLS, NanoBrook Omni, USA). Thermal properties were analyzed by thermogravimetric analysis (TGA, TGA2, Switzerland).

Photothermal Properties of Gold Nanohybrid Composites

The photothermal properties of different nanoparticles were evaluated by exposing nanoparticle solutions to an 808 nm laser while recording temperature changes. Briefly, 1 mL of 400 $\mu\text{g/mL}$ Au-NRs and Au@SiO_2 -HA solutions were irradiated with an 808 nm near-infrared (NIR) lasers at different power densities (1.0, 1.5, 2.0, and 2.5 W/cm^2). Water was used as the control. Real-time photothermal images of the samples were captured using an NIR thermographic camera. Moreover, the photothermal stability of Au@SiO_2 -HA nanoparticles was assessed by repeatedly cycling the NIR laser on and off.

The experimental setup for the NIR photothermal evaluation is detailed as follows: 1 mL of the nanoparticles was placed in a disposable cuvette, positioned 5 cm from the light source. The nanoparticles were irradiated with an 808 nm NIR laser (LR-MFJ808, Changchun Laser Optoelectronics Technology; China) continuously for 10 min at different power densities (1.0, 1.5, 2.0, and 2.5 W/cm²). Temperature changes were recorded in real-time using an infrared thermal imaging camera (DS-2TP31B-3AUF, Hikvision; China), capturing one thermographic image per minute.

Loading of Doxorubicin

Au@SiO₂-HA nanoparticles (5 mg/mL, 10 mL) were mixed with DOX solution (2 mg/mL, 1 mL) and stirred overnight. The mixture was then dialyzed in a dialysis bag for three days, with the dialysate replaced three times daily to obtain Au@SiO₂-HA-DOX. The absorbance of the dialysate at 490 nm was measured using a UV-Vis spectrophotometer, and the encapsulation efficiency (EE) of DOX was calculated using the following equation:

$$EE\% = \left(1 - \frac{W_D}{W_T}\right) \times 100\%$$

where W_T is the total amount of DOX added and W_D is the amount of DOX detected in the dialysate.

In vitro Drug Release Assay

Au@SiO₂-HA-DOX nanoparticles (1 mg/mL) were placed in a dialysis bag and immersed in 30 mL of phosphate buffered saline (PBS) solution at different pH values (5.0, 6.5, 7.4). At predetermined time intervals, 3 mL of the release medium was withdrawn to measure the absorbance at 490 nm, and an equal volume of fresh PBS was added to maintain a constant volume. To assess drug release under oxidative conditions, the nanoparticles were also tested in the presence or absence of H₂O₂. Additionally, effect of NIR light on drug release was assessed by irradiating the nanoparticle suspension with NIR light at various power densities.

In vitro Biocompatibility

Mouse fibroblasts (L929) and human breast cancer cells (MCF-7) were co-cultured with nanoparticles to evaluate biocompatibility and selective targeting. Cells were seeded in 96-well plates at a density of 1×10^5 cells/well and incubated for 24 h. Medium containing Au@SiO₂ and Au@SiO₂-HA nanoparticles at varying concentrations (25, 50, 100, 200, and 400 µg/mL) was then added. For the NIR irradiation group, cells were exposed to an 808 nm laser for 5 min. After 24 h, cell viability was determined using the CCK-8 assay and calculated as follows:

$$\text{Cell viability}(\%) = \frac{OD_{\text{samples}} - OD_{\text{blanks}}}{OD_{\text{Control}} - OD_{\text{blanks}}} \times 100\%$$

where OD_{blanks} , OD_{control} and OD_{samples} represent the optical density values of the blank, control and experimental groups, respectively.

For live/dead staining, L929 cells and MCF-7 cells were seeded in 48-well plates at a density of 1×10^5 cells/well and cultured for 24 h. The medium was then replaced with medium containing 2 µM DOX and Au@SiO₂-HA-DOX, with the NIR irradiation group exposed to an 808 nm laser for 5 min. After 24 h of incubation, cells were stained with a live/dead cell staining kit and observed under a fluorescence microscope.

In vitro Cellular Uptake

Cellular uptake of different nanoparticles was observed using fluorescence staining and laser confocal microscopy. MCF-7 cells were seeded in 24-well plates at a density of 1×10^6 cells/well and cultured with 2 µM DOX and Au@SiO₂-HA-DOX for 4 and 24 h, respectively. The NIR irradiation group was exposed to an 808 nm laser for 5 min. Cells cultured without nanoparticles served as the control group. Following incubation, cells were fixed with glutaraldehyde, washed with PBS, and stained with DAPI for 5 min to visualize nuclei. Cellular uptake was then observed using a laser confocal microscope. In addition, the uptake capacity of MCF-7 cells for nanomedicines was further observed by free HA (5 mg/mL, 5 µL) pretreated with MCF-7 cells for 4 h and co-incubated with nanomedicines for another 24 h.

In vivo Animal Experiments

This study was approved by Shanghai Fourth People's Hospital, Tongji University School of Medicine, Shanghai, China. All animal experiments were reviewed and approved by the Animal Ethics Committee of Shanghai Tongji Biomedical Technology Co., Ltd (Approval No. TJBH 11923102), in accordance with the Guidelines for the Ethical Review of Laboratory Animal Welfare (GB/T 35892–2018) for the care and use of animals. Following a previously described method,⁴² a mouse breast cancer model was established using C57BL/6J mice. Once tumor reached approximately 200 mm³ in volume, the mice were randomly divided into four groups: Control group (PBS treatment group), DOX treatment group, Au@SiO₂-HA-DOX (L-) group (without photothermal treatment), and Au@SiO₂-HA-DOX (L+) group (with photothermal treatment). Mice in the DOX treatment group received an intravenous injection of DOX at a dose of 4 mg/kg, while those in the control group received an equivalent volume of PBS. Mice in the photothermal group were irradiated with 808 nm NIR light for 5 min. Tumor volume (V) was calculated using the formula:

$$V = 1/2 \times \text{length} \times \text{width}^2$$

The relative tumor volume (V/V_0) and relative body weight (M/M_0) changes of mice were recorded, where V and V_0 refer to the real-time tumor volume at each time point and before treatment, respectively, and M and M_0 represent the corresponding body weights. After treatment, the major organs including the heart, liver, spleen, lung, kidney, and tumor tissues were collected and fixed with 4% paraformaldehyde. The tissues were then stained with H&E and observed under an inverted fluorescence microscope.

Statistical Analysis

Data are presented as the mean \pm standard deviation (SD). Unpaired Student's *t* test was used for direct comparisons between two groups. Significance levels are denoted as **P* < 0.05; ***P* < 0.01; ****P* < 0.001.

Results and Discussion

Photothermal-assisted drug therapy has demonstrated significant efficacy in treating solid tumors.⁴³ In this study, GNRs were employed as photothermal agent; however, gold nanorods are known for their poor stability and cytotoxicity.⁴⁴ To address these issues, silica shells were deposited on the surface of GNRs, and HA was grafted onto the hybrid NPs via dynamic borate ester bonds. As depicted in Figure 1A and B, GNRs exhibited a uniformly dispersed rod-like structure. The deposition of SiO₂ and HA on the surface of GNRs resulted in a distinct core-shell structure. The borate structure grafted onto the silica surface can form dynamic covalent cross-linking bonds with the o-hydroxyl groups of HA. This dynamic process gradually coats the GNRs with HA.

The hydrodynamic sizes of Au-NRs and Au@SiO₂ were 132.2 \pm 1.7 nm and 151.5 \pm 2.5 nm, respectively. Upon grafting with HA, the size of Au@SiO₂-HA increased to 202.6 \pm 2.1 nm (Figure 1C). This increase is attributed to the hydrophilic interactions of the polymer, which expand the NPs size upon loading onto the surface. Additionally, the surface potentials of Au-NRs and Au@SiO₂ were -15.8 ± 1.1 mV and -17.2 ± 1.7 mV, respectively, while that of Au@SiO₂-HA was -25.3 ± 2.5 mV (Figure 1D). This indicates the successful grafting of negatively charged HA onto the GNRs.

To further characterize the successful preparation of Au@SiO₂-HA NPs, we employed TGA, FTIR, and UV-Vis spectroscopy to analyze the structures of different NPs. Thermogravimetric analysis revealed that Au@SiO₂-HA-DOX exhibited a mass loss of 23.1% (Figure 2A and B). This significant mass loss can be attributed to the polymer shell structure on the NPs surface and the supported drug molecules. Therefore, the reaction yield of HA conjugated with GNRs was 20.4%. FTIR analysis showed Si-O-Si tensile vibration peaks of Au@SiO₂-HA-DOX NPs at 800 cm⁻¹ and 1100 cm⁻¹, confirming the successful deposition of the silica shell on the GNRs.⁴⁵ Additionally, characteristic absorption peaks of carboxyl groups appeared at 1750 cm⁻¹, indicating successful grafting of HA onto the NPs surface (Figure 2C). UV-Vis spectroscopy revealed two distinct longitudinal and transverse plasmon absorption peaks for GNRs. After successful deposition of silica and HA shells on the GNRs, the characteristic absorption peak of GNRs was significantly

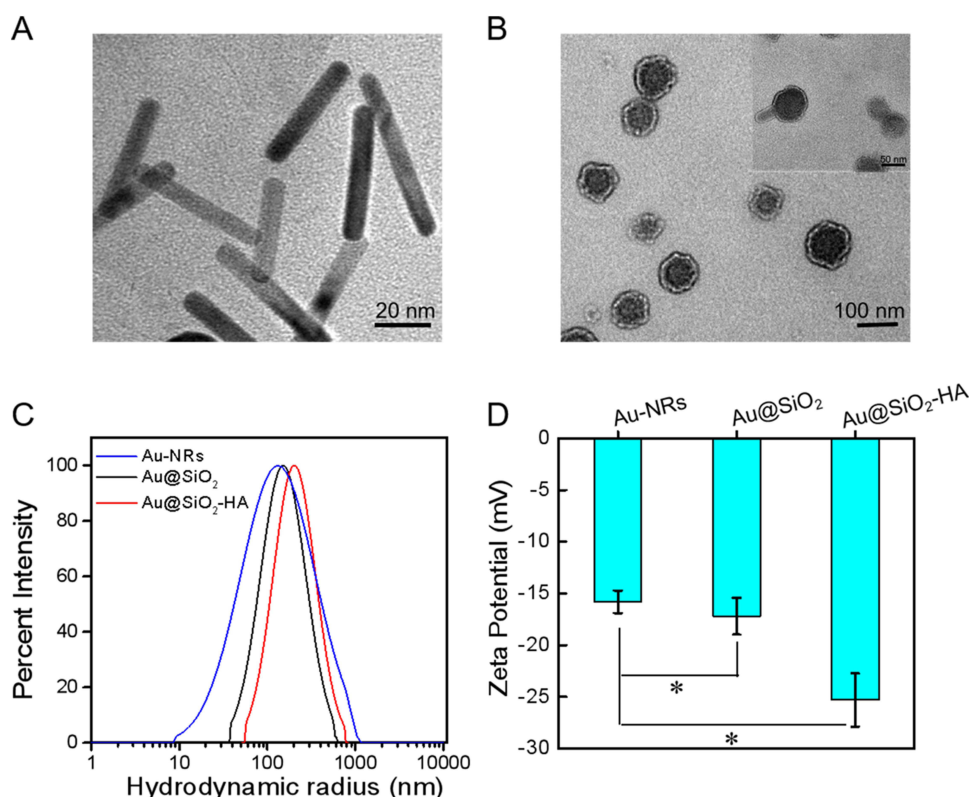


Figure 1 TEM images of (A) Au-NRs and (B) Au@SiO₂-HA (The inset of (B) is the TEM image of silica deposition process on the surface of Au-NRs). Hydrodynamic size (C) and Zeta potential (D) of Au-NRs, Au@SiO₂ and Au@SiO₂-HA. * indicates $P < 0.05$.

Abbreviations: TEM, Transmission electron microscopy; Au-NRs, gold nanorod; Au@SiO₂, gold nanorod/ silicon dioxide, Au@SiO₂-HA, gold nanorod/ silicon dioxide/ hyaluronic acid.

reduced. Upon loading DOX, the Au@SiO₂-HA-DOX NPs exhibited a relatively strong characteristic absorption peak at 490 nm, demonstrating their enhanced loading capacity for DOX (Figure 2D).

GNRs, with tunable aspect ratio and strong surface plasmonic resonance under NIR light irradiation, exhibit significant optical absorption and high photothermal conversion efficiency.⁴⁶ In this study, different shell layers were deposited on the surface of GNRs to further investigate their photothermal properties. When irradiated with 808 nm NIR light, the temperature of Au@SiO₂-HA NPs rapidly increased by 31 °C within 10 min, while the aqueous control solution exhibited no significant temperature change (Figure 3A). Moreover, the optical density and irradiation time of NIR light significantly influenced the temperature change of the Au@SiO₂-HA NPs solution. At a concentration of 400 µg/mL, irradiation of Au@SiO₂-HA NPs with 1.0 W/cm² for 10 min resulted in a temperature increase of 30 °C (Figure 3B and C). Au@SiO₂-HA also demonstrated excellent photothermal stability during three cycles of laser on/off irradiation (Figure 3D).

Real-time near-infrared thermal imaging showed that the temperature of the aqueous solution remained virtually unchanged when irradiated with an 808 nm laser at a power density of 2.0 W/cm² for 10 min. In contrast, both Au-NRs and Au@SiO₂-HA NPs exhibited rapid temperature increases. Notably, Au@SiO₂-HA NPs displayed the most pronounced thermal effect and the largest temperature change (Figure 4). These findings are consistent with the previously observed temperature changes results. Therefore, Au@SiO₂-HA NPs exhibit superior photothermal stability and imaging performance.

Drug Loading and Responsive Drug Release Properties of the Nanoparticles

The effective loading and slow controlled release of drugs by nanocarriers are key to enhancing the utilization and therapeutic efficiency of cancer drugs.⁴⁷ The loading efficiency of DOX by Au@SiO₂-HA NPs was significantly enhanced compared to unmodified Au@SiO₂. Specifically, the loading efficiency of unmodified Au@SiO₂ for DOX

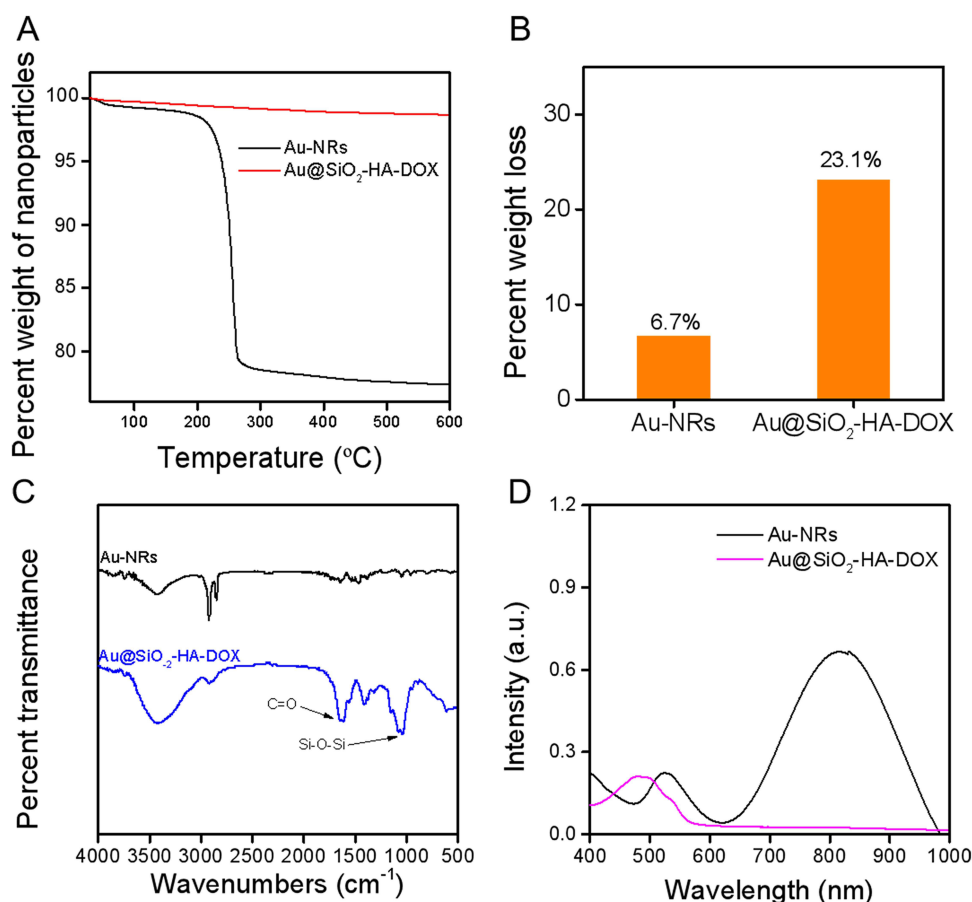


Figure 2 Microstructure characterization of different nanoparticles. **(A)** Thermogravimetric analysis of Au-NRs and Au@SiO₂-HA-DOX. **(B)** Corresponding quantitative data for thermogravimetric analysis. **(C)** FTIR spectra and **(D)** UV-Vis spectra of Au-NRs and Au@SiO₂-HA-DOX, respectively.

Abbreviations: Au-NRs, gold nanorod, Au@SiO₂-HA-DOX, gold nanorod/silicon dioxide/hyaluronic acid/doxorubicin, FTIR, Fourier Transform infrared spectroscopy, UV-Vis, Ultraviolet-visible spectroscopy.

was $52.3\% \pm 3.5\%$, while that of Au@SiO₂-HA increased to $65.9\% \pm 2.7\%$ (Figure 5A). This improvement is likely due to the negatively charged HA encapsulating the positively charged DOX molecules within the NPs. Additionally, the colloidal stability of the nanomedicine was evaluated by monitoring the surface potential of the NPs in PBS solutions at different pH values. The surface potential remained relatively stable across various pH conditions, indicating that the nanomedicine exhibited good colloidal stability (Figure 5B).

One of the critical aspects of nanomedicine in tumor therapy is the long-acting and controlled release of anticancer drugs in tumor tissues.⁴⁸ Tumor cells exhibit specific changes that create physiological conditions distinct from those of normal tissues, such as low pH, oxidative stress, and elevated enzyme expression.⁴⁹ In this study, Free DOX released over 80% of the drug within 4 h when placed in a solution with a pH of 7.4. However, Au@SiO₂-HA-DOX demonstrated a sustainable drug release behavior up to 48 h (Figure 5C). Notably, the release behavior of Au@SiO₂-HA-DOX varied with different pH values. At pH 5.0, the cumulative release rate reached $72 \pm 2.9\%$ within 48 h (Figure 5D), attributable to the responsive cleavage of HA-borate complex. Additionally, in the elevated H₂O₂ levels within tumors, the dynamic boronate cross-links are efficiently hydrolyzed to boric acid and diol. Our results showed that Au@SiO₂-HA-DOX exhibited a dose-dependent drug release behavior in response to H₂O₂ with a cumulative DOX release reaching $87.3 \pm 3.9\%$ at a 1.0 mM H₂O₂ concentration (Figure 5E).

In addition to responding to the internal stimulation from the tumor environment, the effective release of drugs can be achieved using external stimulation. GNRs possess excellent plasmon resonance properties, enabling them to generate heat in response to NIR light stimulation.⁵⁰ When NIR light was applied at intervals in a PBS solution at pH 5.0, the

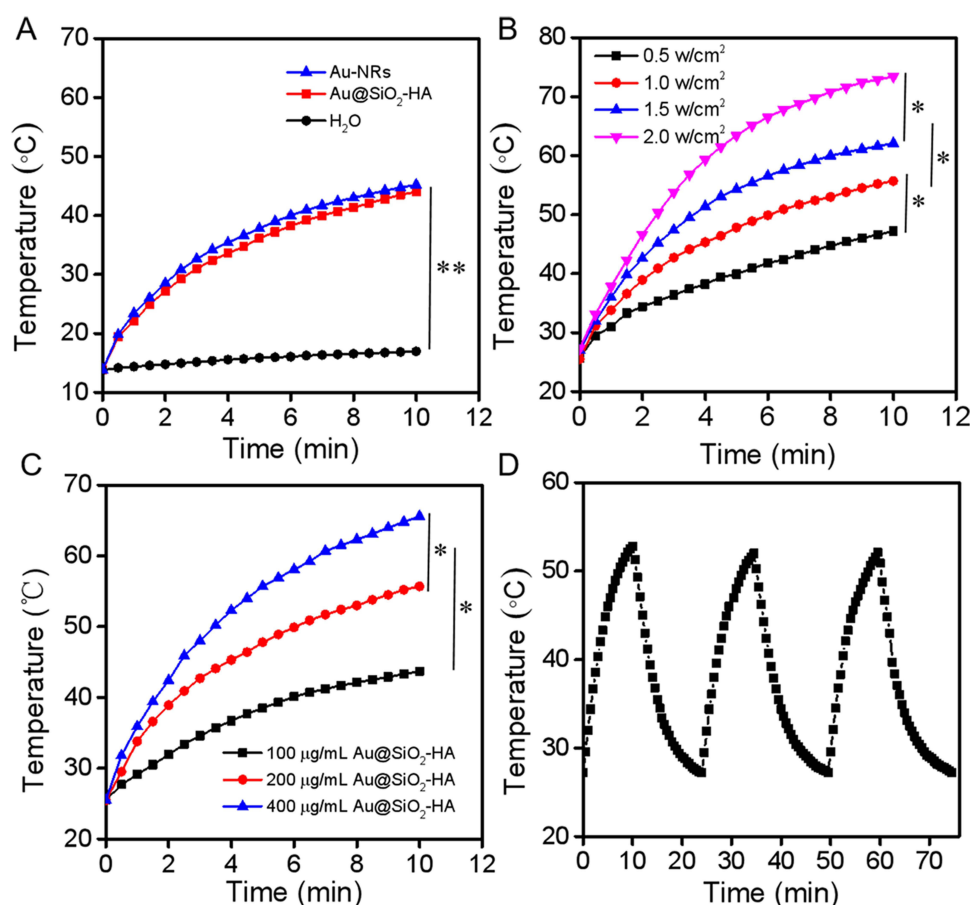


Figure 3 Photothermal properties of different materials. (A) Temperature change curves of different materials. (B) Temperature change curves of Au@SiO₂-HA with different laser power densities (0.5, 1.0, 1.5 and 2.0 W/cm²). (C) Temperature change curves of Au@SiO₂-HA with different concentration (100, 200, 400 µg/mL). (D) Cyclic heating profile of Au@SiO₂-HA for three on/off cycles. * indicates P thermal image of H₂O, Au-NRs, and Au@SiO₂-HA.

Notes: . < 0.05, whereas ** indicates P < 0.01.

Abbreviations: H₂O, water, Au-NRs, gold nanorod, Au@SiO₂-HA, gold nanorod/silicon dioxide/hyaluronic.

Au@SiO₂-HA-DOX NPs exhibited a responsive increase in drug release, resulting in a cumulative drug release increase of $9.0 \pm 1.4\%$ (Figure 5F). The dynamic and responsive borate structure design, combined with the unique properties of gold nanorods, ensures the responsive and sustained release of anti-tumor drugs in tumor tissues.

The cytotoxicity of nanocarriers is crucial for their in vivo application. After 24 h of co-culture with Au@SiO₂-HA and AuNRs, the survival rate of L929 cells remained above 80%, even at a concentration of 300 µg/mL (Figure 6A). Compared to AuNRs, Au@SiO₂-HA exhibited a greater ability to promote cell growth, indicating that polymer surface modifications can enhance the biocompatibility of NPs. Additionally, the effect of NIR irradiation on L929 cells was evaluated. After 24 h of co-culture with Au@SiO₂-HA NPs, green fluorescence was evident, while red fluorescence was virtually absent. Following irradiation with 808 nm NIR light, no red fluorescence was observed, and cell morphology remained normal, confirming that NIR irradiation does not affect the basic physiological functions of cells (Figure 6B).

The cytotoxicity of Au@SiO₂-HA NPs was evaluated to determine their potential for in vivo applications. MCF-7 cells were co-cultured with free DOX and Au@SiO₂-HA-DOX for 24 h. Both free DOX and Au@SiO₂-HA-DOX exhibited concentration-dependent cytotoxicity. At a DOX concentration of 2 µM, the viability of cancer cells treated with free DOX exceeded 70%, whereas treatment with Au@SiO₂-HA-DOX resulted in a significantly reduced viability of $33.5 \pm 1.9\%$ (Figure 7A). This indicates that Au@SiO₂-HA-DOX has a lower effective tumor inhibitory concentration compared to free DOX. The IC₅₀ values for DOX and Au@SiO₂-HA-DOX were 2.91 µM and 1.36 µM, respectively, further confirming the enhanced efficacy of the nanocarrier in killing cancer cells at lower drug concentrations.

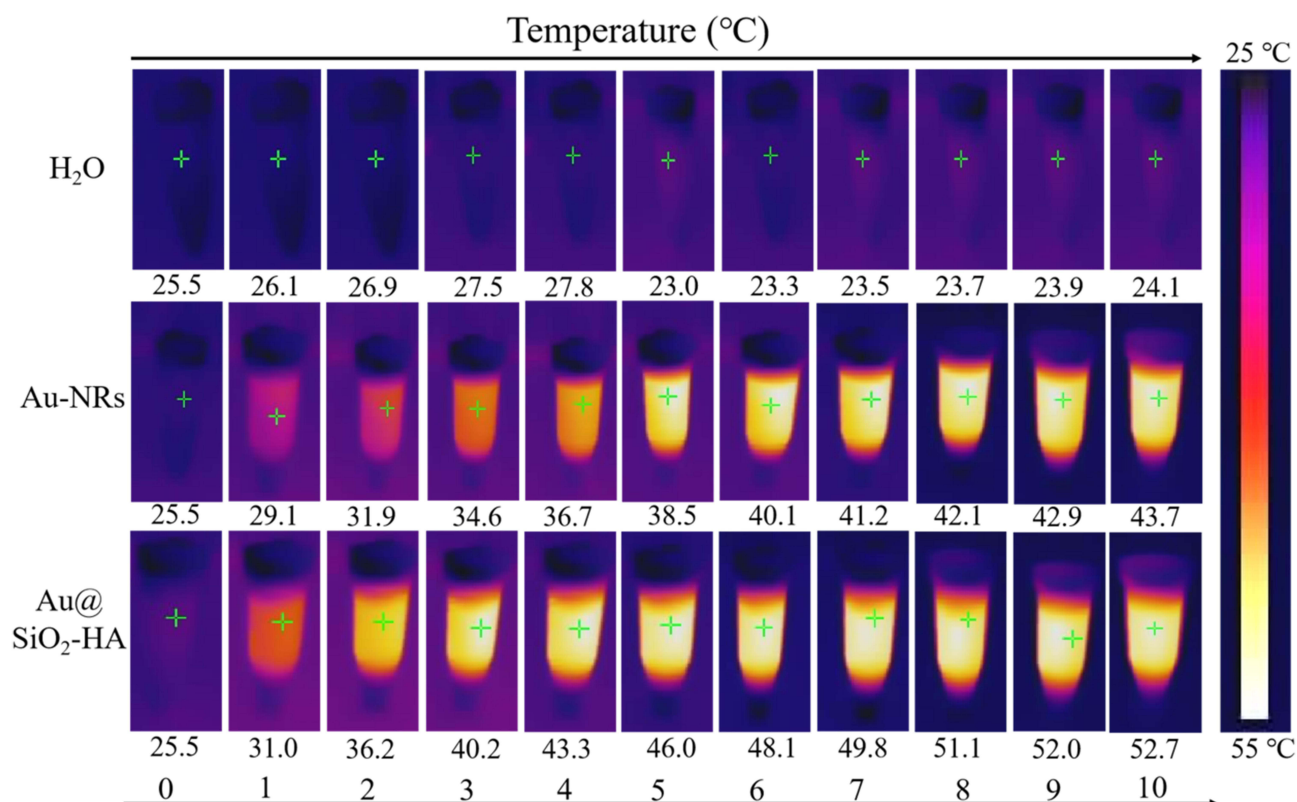


Figure 4 Real time NIR thermal image of H₂O, Au-NRs, and Au@SiO₂-HA.

Abbreviations: H₂O, water; Au-NRs, gold nanorod; Au@SiO₂-HA, gold nanorod/ silicon dioxide/hyaluronic acid.

(Figure 7B). Live/dead cell staining results showed that at a DOX concentration of 2.0 μ M, the Au@SiO₂-HA-DOX group exhibited more red fluorescence (indicating dead cells) than the Free DOX group, demonstrating the superior cytotoxicity of the nanocarrier. When exposed to NIR light irradiation, the number of dead cells remained unchanged in the free DOX group, whereas the nanocarrier group showed a significant increase in the dead cell distribution, along with irregular cell morphology and disrupted cell structure (Figure 7C). These results demonstrate that Au@SiO₂-HA nanocarriers exhibit enhanced cytotoxicity against cancer cells at lower drug concentrations compared to free DOX.

The cellular uptake of nanomedicines was analyzed using confocal laser scanning microscopy. After co-culture with cancer cells for 4 h, cells treated with Au@SiO₂-HA-DOX exhibited pronounced red fluorescence (indicative of DOX), whereas the control group displayed negligible red fluorescence (Figure 8A), which indicates that Au@SiO₂-HA-DOX can rapidly enter cells within 4 h. Upon NIR light irradiation, the red fluorescence intensity increased slightly. Quantitative analysis revealed that the intracellular DOX fluorescence intensity after NIR irradiation was 1.3 times that of the control group (Figure 8B). This enhancement may be attributed to increased cell permeability induced by NIR light, facilitating greater uptake of the nanomedicine by cancer cells. After 24 h of co-culture, weak red fluorescence was observed in the DOX group, indicating that small-molecule drugs enter cells via passive diffusion, a time-dependent process with low drug utilization efficiency (Figure 8C). In contrast, the red fluorescence in the Au@SiO₂-HA-DOX group was more intense after NIR irradiation, with a fluorescence intensity 1.7 times that of the DOX group. Moreover, after pre-incubation of MCF-7 cells using free HA and then co-incubation with nanoparticles, the intracellular fluorescence intensity was significantly reduced (Figure 8D). These findings suggest that HA can target the CD44 receptor on cancer cells, effectively promoting the enrichment of Au@SiO₂-HA-DOX NPs around cancer cells, while NIR stimulation enhances the uptake of NPs by cancer cells. These results demonstrate that Au@SiO₂-HA-DOX is an effective carrier for anticancer drug delivery, significantly improving the uptake and utilization efficiency of drugs by cancer cells.

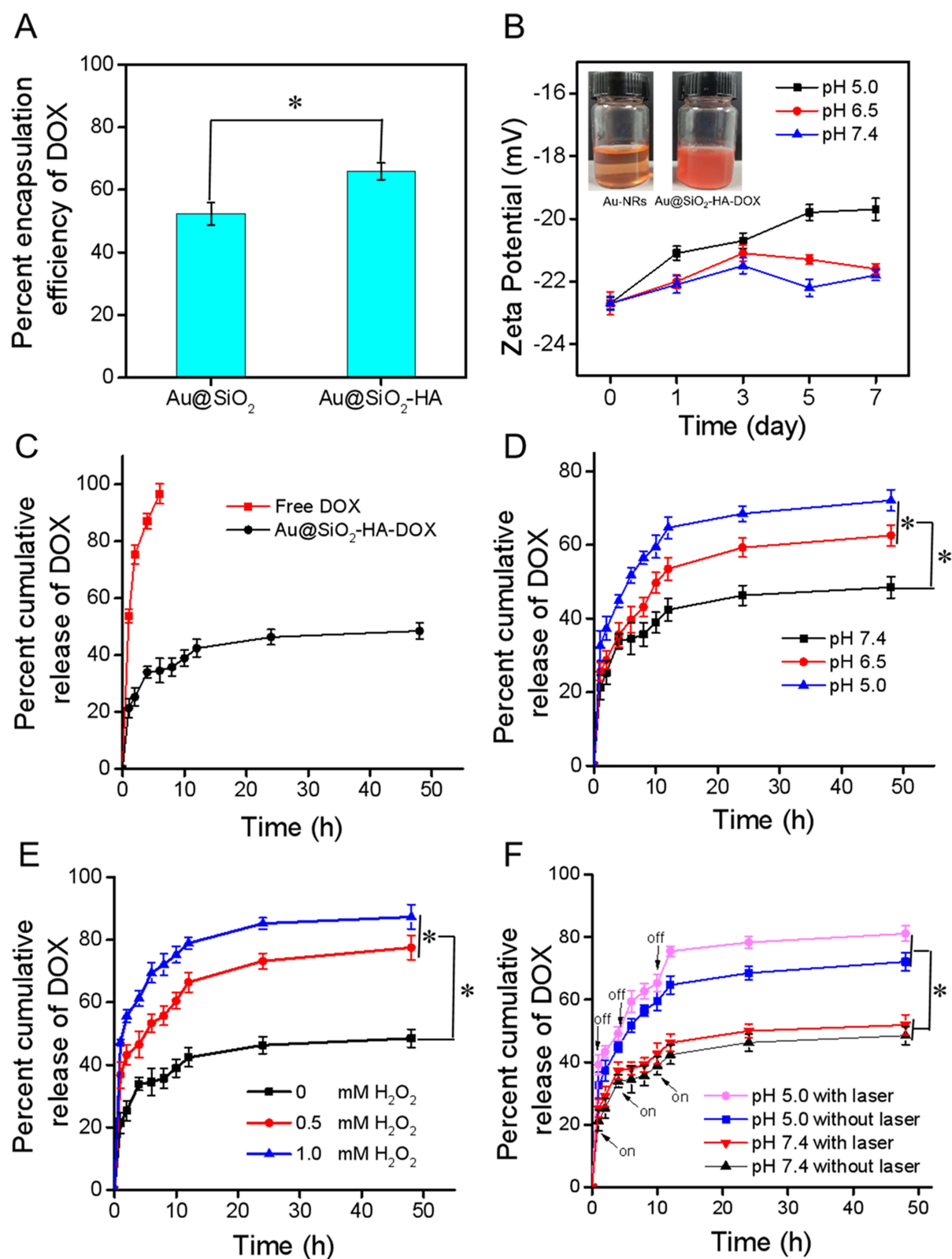


Figure 5 Study of drug loading and drug release behavior of different materials. **(A)** Drug encapsulation efficiency of Au@SiO₂ and Au@SiO₂-HA. **(B)** The surface charge of Au@SiO₂-HA-DOX nanoparticles in PBS (5.0, 6.5, 7.4) solution for different days (The inset of **(B)** is an image of Au-NRs and Au@SiO₂-HA-DOX dispersed in PBS for 7 days). **(C)** DOX release curve of Free DOX and Au@SiO₂-HA-DOX. DOX release curve from Au@SiO₂-HA-DOX **(D)** at pH 5.0, 6.5, and 7.4; **(E)** in different concentration of H₂O₂ (0, 0.5 mm, 1.0 mm). **(F)** DOX release curves of Au@SiO₂-HA-DOX with or without near-infrared light. * indicates P < 0.05.

Abbreviations: Au-NRs, gold nanorod; Au@SiO₂, gold nanorod/ silicon dioxide; Au@SiO₂-HA, gold nanorod/ silicon dioxide/hyaluronic acid; Au@SiO₂-HA-DOX, gold nanorod/silicon dioxide/hyaluronic acid/doxorubicin; PBS, phosphate-buffered sodium; DOX, doxorubicin; H₂O₂, Hydrogen peroxide.

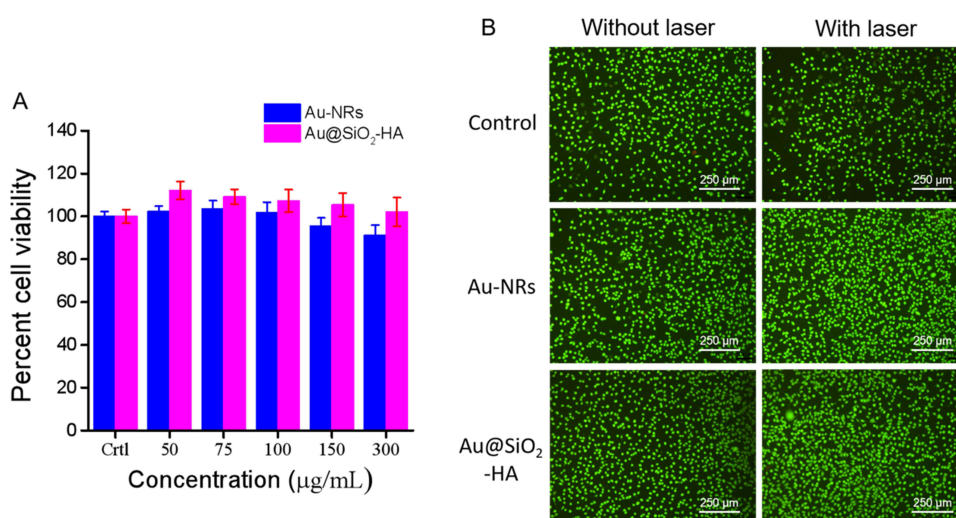


Figure 6 In vitro biocompatibility of (A) Au-NRs and Au@SiO₂-HA. (B) Live/dead staining images of L929 cells incubated with Au-NRs and Au@SiO₂-HA with or without NIR irradiation.

Abbreviations: Au-NRs, gold nanorod; Au@SiO₂-HA, gold nanorod/ silicon dioxide/hyaluronic acid; NIR, near-infrared.

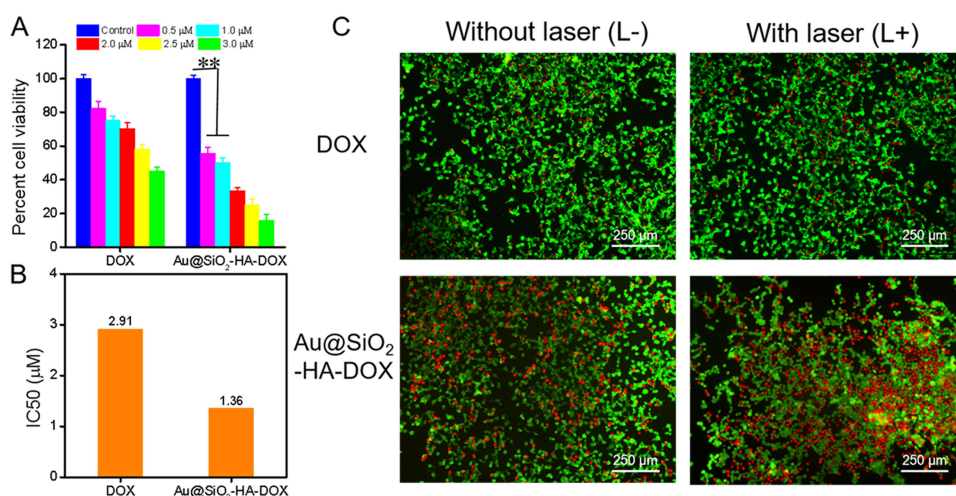


Figure 7 Drug loading and drug release behavior of different materials. (A) Cell viability of MCF-7 cells incubated with DOX and Au@SiO₂-HA-DOX at different concentration. (B) IC₅₀ value of DOX and Au@SiO₂-HA-DOX. (C) Live/dead staining image of MCF-7 cells treated with DOX and Au@SiO₂-HA-DOX with or without NIR irradiation. ** indicates $P < 0.01$.

Abbreviations: MCF-7, Michigan Cancer Foundation-7; DOX, doxorubicin; Au@SiO₂-HA-DOX, gold nanorod/silicon dioxide/hyaluronic acid/doxorubicin; IC₅₀, Half maximal inhibitory concentration; NIR, near-infrared; L-, without laser; L+, with laser.

The in vivo anti-tumor potential of nanomedicine was assessed by tumor growth analysis. Tumors volume in the control group exhibited significant and continuous growth, whereas those in the DOX-treated group showed moderate inhibition, likely due to the partial passive diffusion of DOX into tumor tissues, where it disrupts the DNA double helix structure of cancer cells. In contrast, the Au@SiO₂-HA-DOX group demonstrated considerable tumor growth suppression, with the most pronounced effect observed under NIR light irradiation. This enhancement is ascribed to the active targeting ability of HA, which facilitates selective accumulation and high intracellular uptake of the drug in cancer cells, thereby improving anticancer activity (Figure 9A). In addition, mice in the free DOX group exhibited slow weight gain, likely due to systemic toxicity, while those in the nanomedicine group maintained stable weight gain, indicating reduced toxicity (Figure 9B).

After 12 days of treatment, tumor tissues were collected. The results indicated that the photothermal treatment group had the smallest tumor size and weight, consistent with experimental measurements, thus confirming the efficacy of

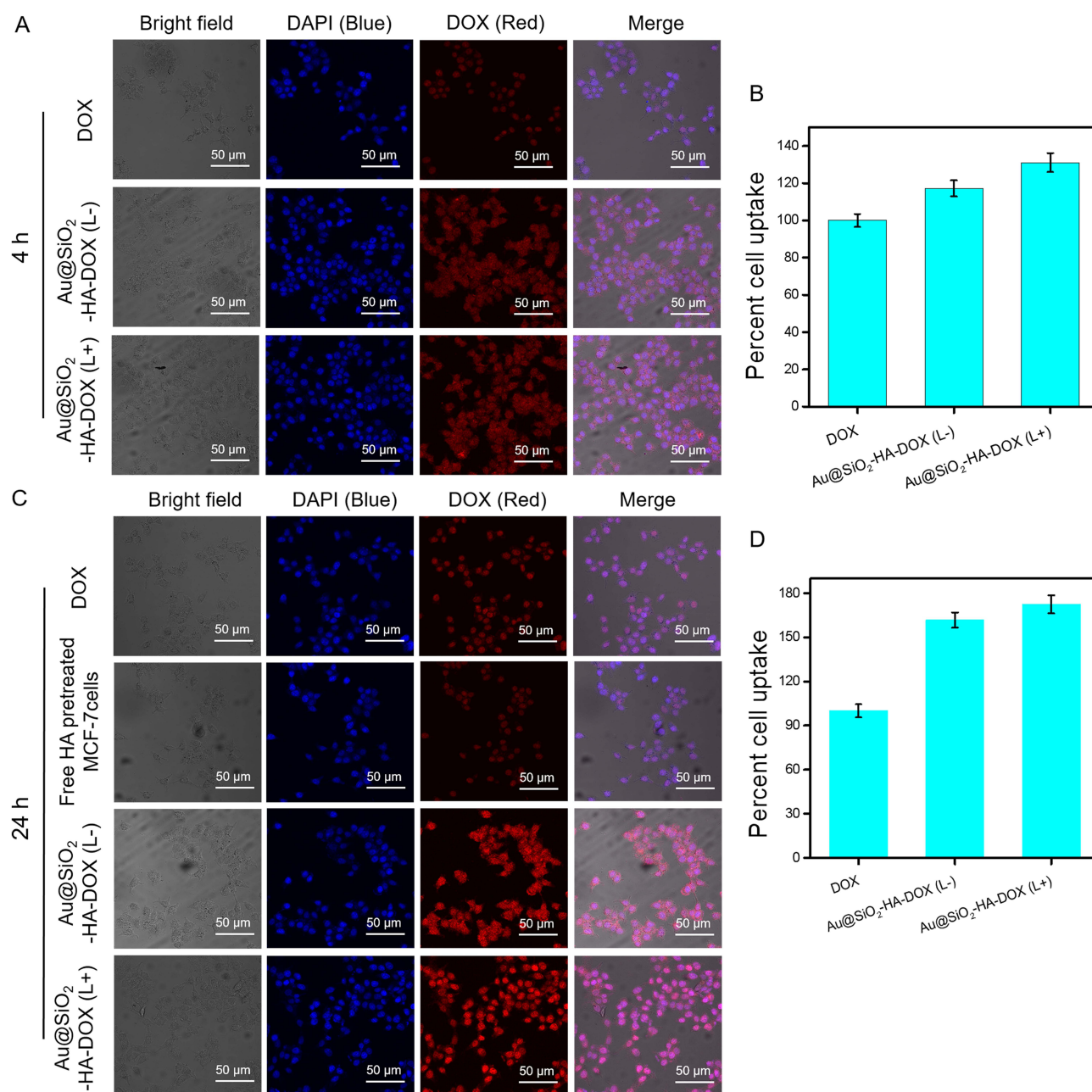


Figure 8 Fluorescence microscopy images of MCF-7 cells after treated with DOX or Au@SiO₂-HA-DOX for (A) 4 h and (B) 24 h. The relative fluorescence intensity of MCF-7 cells after (C) 4 h and (D) 24 h.

Abbreviations: MCF-7, Michigan Cancer Foundation-7; DOX, doxorubicin; Au@SiO₂-HA-DOX, gold nanorod/silicon dioxide/hyaluronic acid/doxorubicin; L-, without laser; L+, with laser.

nanomaterial-assisted photothermal therapy in inhibiting tumor growth (Figure 9C and D). Histological analysis of tumor tissues showed closely packed and regular tumor cells in the control group, with only a few dead cells in the DOX-treated group. In contrast, the photothermal treatment group exhibited ruptured tumor cells with evident apoptosis, demonstrating that nanomedicine can effectively enter tumor tissues via NIR stimulation and induce cell death (Figure 9E).

The in vivo biosafety of the nanomedicine was evaluated through histological analysis of major organs from mice. No significant infiltration of inflammatory cells was observed in the major metabolic organs (heart, liver, spleen, and lung), and the cellular structures remained intact (Figure 10). These findings indicate that the cytotoxicity of the nanomaterials in non-tumor tissues is minimal, demonstrating the excellent biocompatibility of the nanomedicine.

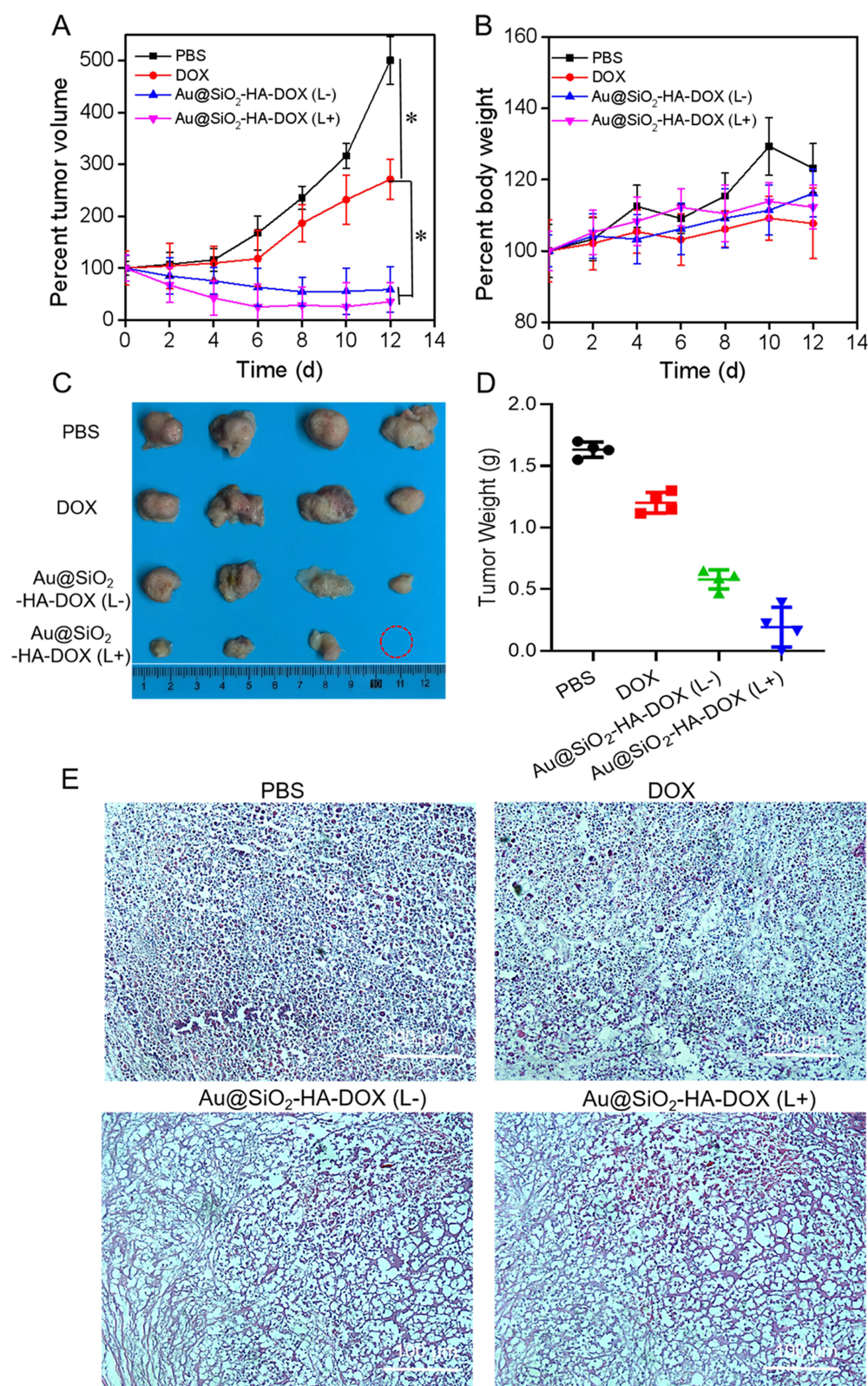


Figure 9 In vivo anti-tumor effects of nanomedicines. **(A)** Relative tumor volume and **(B)** Relative body weight of C57BL/6J mice after treated with different materials. **(C)** The image of resected tumors and **(D)** the tumor weight. **(E)** H&E stained slices of tumor tissues.* indicates $P < 0.05$.

Abbreviations: H&E, hematoxylin-eosin staining; L-, without laser; L+, with laser.

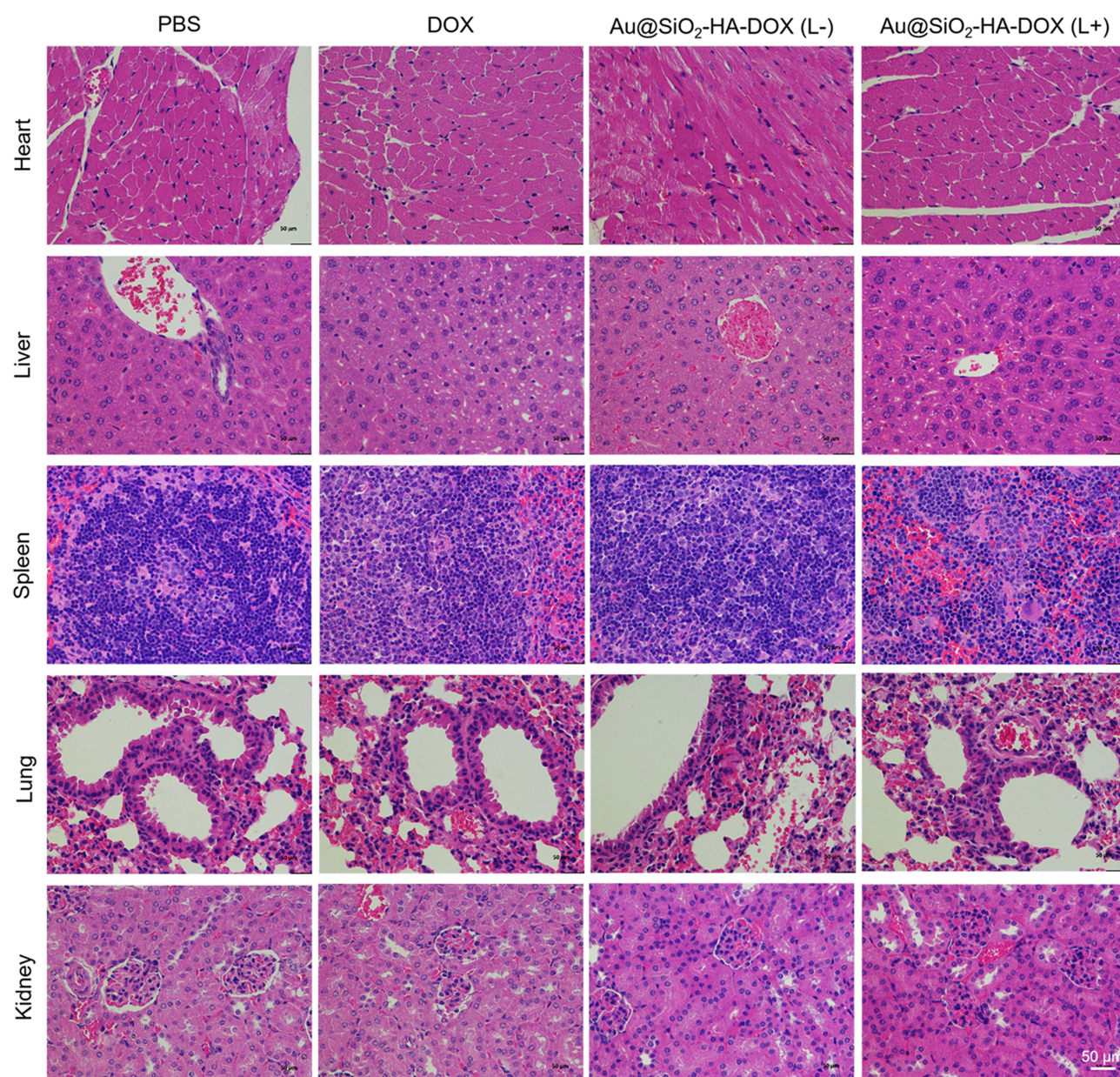


Figure 10 H&E staining of vital organs after treated with PBS, DOX; Au@SiO₂-HA-DOX (L-) and Au@SiO₂-HA-DOX (L+).

Abbreviations: PBS, phosphate-buffered sodium; DOX, doxorubicin; Au@SiO₂-HA-DOX, gold nanorod/silicon dioxide/hyaluronic acid/doxorubicin; H&E, hematoxylin-eosin staining; L-, without laser; L+, with laser.

Conclusion

In this study, we successfully developed a multifunctional responsive gold nanorod-based hybrid nanoplatform capable of efficiently loading anticancer drugs and supporting controlled release within the tumor microenvironment. The dynamic borate design, responsive to both exogenous near-infrared light stimulation and endogenous reactive oxygen species, facilitates the precise and stimuli-triggered release of doxorubicin from the nanocarriers. This innovative approach not only improves the specificity of anticancer treatment but also offers a promising strategy for designing materials tailored to the tumor microenvironment. Our findings indicate that this nanoplatform holds significant potential for enhancing the clinical efficacy of antitumor drugs. However, the optimization of nanodrug design for targeted delivery and precise control of drug release remains a critical area that requires further investigation. Future research should focus on improving the targeting efficiency through the incorporation of tumor-specific ligands and the exploration of nanoplatform in diverse tumor models.

Acknowledgments

This work was funded by the scientific research project of the Hongkou District Health Committee of Shanghai (No. 2302-09, 2403-09), by the research project of Shanghai Fourth People's Hospital (sykyqd-00703 & xkzt-2022-1019, 2020-1020) and Beijing Dadi Medical Charity Foundation. Hubei Provincial Administration of Traditional Chinese Medicine Scientific Research Program in Traditional Chinese Medicine (ZY2025L044).

Disclosure

The authors declare no conflicts of interest in this work.

References

1. Aikins ME, Xu C, Moon JJ. Engineered nanoparticles for cancer vaccination and immunotherapy. *Acc Chem Res.* 2020;53(10):2094–2105. doi:10.1021/acs.accounts.0c00456
2. Meng X, Wang X, Zhang Z, Song L, Chen J. Recent advancements of nanomedicine in breast cancer surgery. *Int J Nanomed.* 2024;19:14143–14169. doi:10.2147/ijn.S494364
3. Qu X, Zhou D, Lu J, Qin D, Zhou J, Liu H-J. Cancer nanomedicine in preoperative therapeutics: nanotechnology-enabled neoadjuvant chemotherapy, radiotherapy, immunotherapy, and phototherapy. *Bioact Mater.* 2023;24:136–152. doi:10.1016/j.bioactmat.2022.12.010
4. Wei G, Wang Y, Yang G, Wang Y, Ju R. Recent progress in nanomedicine for enhanced cancer chemotherapy. *Theranostics.* 2021;11(13):6370–6392. doi:10.7150/thno.57828
5. Kiaee G, Dimitrakakis N, Sharifzadeh S, et al. Laponite-based nanomaterials for drug delivery. *Adv Healthcare Mater.* 2022;11(7):2102054. doi:10.1002/adhm.202102054
6. Bedhafi T, Idoudi S, Alhams AA, et al. Applications of polydopaminic nanomaterials in mucosal drug delivery. *J Control Release.* 2023;353:842–849. doi:10.1016/j.jconrel.2022.12.037
7. Shang Y, Zhang H, Cheng Y, et al. Fluorescent imaging-guided chemo- and photodynamic therapy of hepatocellular carcinoma with HCPT@NMOFs-RGD nanocomposites. *Int J Nanomed.* 2022;17:1381–1395. doi:10.2147/ijn.S353803
8. Sun Q, Ojha T, Kiessling F, Lammers T, Shi Y. Enhancing tumor penetration of nanomedicines. *Biomacromolecules.* 2017;18(5):1449–1459. doi:10.1021/acs.biomac.7b00068
9. Zhou Q, Li J, Xiang J, et al. Transcytosis-enabled active extravasation of tumor nanomedicine. *Adv Drug Delivery Rev.* 2022;189:114480. doi:10.1016/j.addr.2022.114480
10. Guo Y, Hu P, Shi J. Nanomedicine Remodels Tumor Microenvironment for Solid Tumor Immunotherapy. *J Am Chem Soc.* 2024;146(15):10217–10233. doi:10.1021/jacs.3c14005
11. Zhang Y, Chen W, Yang C, Fan Q, Wu W, Jiang X. Enhancing tumor penetration and targeting using size-minimized and zwitterionic nanomedicines. *J Control Release.* 2016;237:115–124. doi:10.1016/j.jconrel.2016.07.011
12. Xiong P, Wei X, Zhou L, et al. Near-Infrared light-triggered MXene nanocomposite for tumor-specific mild photothermal-enhanced chemodynamic therapy. *Adv Funct Mater.* 2024;34(44):2405124. doi:10.1002/adfm.202405124
13. Alamdari SG, Amini M, Jalilzadeh N, et al. Recent advances in nanoparticle-based photothermal therapy for breast cancer. *J Control Release.* 2022;349:269–303. doi:10.1016/j.jconrel.2022.06.050
14. Hu Y, Zhou Y, Li K, Zhou D. Recent advances in near-infrared stimulated nanohybrid hydrogels for cancer photothermal therapy. *Biomater Sci.* 2024;12(18):4590–4606. doi:10.1039/D4BM00662C
15. Farivar N, Khazamipour N, Roberts ME, et al. Pulsed photothermal therapy of solid tumors as a precondition for immunotherapy. *Small.* 2024;20(32):2309495. doi:10.1002/smll.202309495
16. Cao Y, Jin L, Zhang S, et al. Blood-brain barrier permeable and multi-stimuli responsive nanoplatform for orthotopic glioma inhibition by synergistic enhanced chemo-/chemodynamic/photothermal/starvation therapy. *Eur J Pharm Sci.* 2023;180:106319. doi:10.1016/j.ejps.2022.106319
17. Shen S, Qiu J, Huo D, Xia Y. Nanomaterial-enabled photothermal heating and its use for cancer therapy via localized hyperthermia. *Small.* 2024;20(7):2305426. doi:10.1002/smll.202305426
18. El-Sayed N, Elbadri K, Correia A, Santos HA. Polyethylene glycol-stabilized gold nanostars-loaded microneedles for photothermal therapy of melanoma. *Adv Mater Technol.* 2023;8(24):2301159. doi:10.1002/admt.202301159
19. Wang F, Wu Q, Jia G, et al. Black phosphorus/MnO₂ nanocomposite disrupting bacterial thermotolerance for efficient mild-temperature photothermal therapy. *Adv Sci.* 2023;10(30):2303911. doi:10.1002/advs.202303911
20. Zhang Y, Han X, Nie G. Responsive and activable nanomedicines for remodeling the tumor microenvironment. *Nat Protocols.* 2021;16(1):405–430. doi:10.1038/s41596-020-00421-0
21. Liu J, Li X, Li Y, Gong Q, Luo K. Metformin-based nanomedicines for reprogramming tumor immune microenvironment. *Theranostics.* 2025;15(3):993–1016. doi:10.7150/thno.104872
22. Shi M, Fu Z, Pan W, et al. A protein-binding molecular photothermal agent for tumor ablation. *Angew Chem Int Ed.* 2021;60(24):13564–13568. doi:10.1002/anie.202101009
23. Chen G, Yang Z, Yu X, et al. Intratumor delivery of amino-modified graphene oxide as a multifunctional photothermal agent for efficient antitumor phototherapy. *J Colloid Interface Sci.* 2023;652:1108–1116. doi:10.1016/j.jcis.2023.08.126
24. Xie Z, Wang D, Fan T, et al. Black phosphorus analogue tin sulfide nanosheets: synthesis and application as near-infrared photothermal agents and drug delivery platforms for cancer therapy. *J Mater Chem B.* 2018;6(29):4747–4755. doi:10.1039/C8TB00729B
25. Marin R, Skripka A, Besteiro LV, et al. Highly efficient copper sulfide-based near-infrared photothermal agents: exploring the limits of macroscopic heat conversion. *Small.* 2018;14(49):1803282. doi:10.1002/smll.201803282
26. Sun L, Li Z, Li Z, et al. Design and mechanism of core-shell TiO₂ nanoparticles as a high-performance photothermal agent. *Nanoscale.* 2017;9(42):16183–16192. doi:10.1039/C7NR02848B

27. Almada M, Leal-Martínez BH, Hassan N, et al. Photothermal conversion efficiency and cytotoxic effect of gold nanorods stabilized with chitosan, alginate and poly(vinyl alcohol). *Mater Sci Eng C*. 2017;77:583–593. doi:10.1016/j.msec.2017.03.218
28. Nejabat M, Samie A, Ramezani M, Alibolandi M, Abnous K, Taghdisi SM. An overview on gold nanorods as versatile nanoparticles in cancer therapy. *J Control Release*. 2023;354:221–242. doi:10.1016/j.jconrel.2023.01.009
29. Kim MJ, Jung DH, Lee CY, Hong S, Heo JH, Lee JH. Structurally engineered silica shells on gold nanorods for biomedical applications. *Small Struct*. 2023;4(9):2300047. doi:10.1002/ssr.202300047
30. Gomez KE, Wu F, Keysar SB, et al. Cancer cell CD44 mediates macrophage/monocyte-driven regulation of head and neck cancer stem cells. *Cancer Res*. 2020;80(19):4185–4198. doi:10.1158/0008-5472.CAN-20-1079
31. Ding L, Jiang Y, Zhang J, Klok H-A, Zhong Z. pH-sensitive coiled-coil peptide-cross-linked hyaluronic acid nanogels: synthesis and targeted intracellular protein delivery to CD44 positive cancer cells. *Biomacromolecules*. 2018;19(2):555–562. doi:10.1021/acs.biomac.7b01664
32. Wu C, Mao Y, Wang X, Li P, Tang B. Deep-tissue fluorescence imaging study of reactive oxygen species in a tumor microenvironment. *Anal Chem*. 2022;94(1):165–176. doi:10.1021/acs.analchem.1c03104
33. Yu X, Yang X, Horte S, Kizhakkedathu JN, Brooks DE. A pH and thermosensitive choline phosphate-based delivery platform targeted to the acidic tumor microenvironment. *Biomaterials*. 2014;35(1):278–286. doi:10.1016/j.biomaterials.2013.09.052
34. Moradi Kashkooli F, Soltani M, Souri M. Controlled anti-cancer drug release through advanced nano-drug delivery systems: static and dynamic targeting strategies. *J Control Release*. 2020;327:316–349. doi:10.1016/j.jconrel.2020.08.012
35. Gong L, Kwong DL-W, Dai W, et al. Comprehensive single-cell sequencing reveals the stromal dynamics and tumor-specific characteristics in the microenvironment of nasopharyngeal carcinoma. *Nat Commun*. 2021;12(1):1540. doi:10.1038/s41467-021-21795-z
36. Xu J, Song M, Fang Z, Zheng L, Wang J, Liu K. A chemioimmunotherapy-based strategy to enhance tumor therapy by cross-linking a novel size-variable nanocluster via a bifunctional peptide. *Mater Des*. 2023;233:112232. doi:10.1016/j.matdes.2023.112232
37. Bai Y, Hua J, Zhao J, et al. A Silver-induced absorption red-shifted dual-targeted nanodiagnosis-treatment agent for NIR-II photoacoustic imaging-guided photothermal and ROS simultaneously enhanced immune checkpoint blockade antitumor therapy. *Adv Sci*. 2024;11(11):2306375. doi:10.1002/advs.202306375
38. Zuo Y, Li P, Wang W-J, et al. Tumor site-specific in vivo theranostics enabled by microenvironment-dependent chemical transformation and self-amplifying effect. *Adv Sci*. 2024;12(4):2409506. doi:10.1002/advs.202409506
39. Wang S, Gao Y, Dong L, Chen P, Liu W, Yang L. Cartilage-targeting and inflammatory-responsive nanocarriers for effective osteoarthritis treatment via reactive oxygen species scavenging and anti-angiogenesis. *J Mater Sci Technol*. 2023;143:30–42. doi:10.1016/j.jmst.2022.08.048
40. Liu Y, Zhu M, Ou J, et al. Multi-responsive sodium hyaluronate/tannic acid hydrogels with ROS scavenging ability promote the healing of diabetic wounds. *Int J Biol Macromol*. 2024;278:134896. doi:10.1016/j.ijbiomac.2024.134896
41. Wang S, Zhao X, Wang S, Qian J, He S. Biologically inspired polydopamine capped gold nanorods for drug delivery and light-mediated cancer therapy. *ACS Appl Mater Interfaces*. 2016;8(37):24368–24384. doi:10.1021/acsami.6b05907
42. Zhou D, Liu S, Hu Y, et al. Tumor-mediated shape-transformable nanogels with pH/redox/enzymatic-sensitivity for anticancer therapy. *J Mater Chem B*. 2020;8(17):3801–3813. doi:10.1039/D0TB00143K
43. Tang X, Zhu Y, Duan D, et al. Anionic solid solution MXene for low-dosage NIR-II tumor photothermal therapy. *Adv Funct Mater*. 2023;33(42):2305965. doi:10.1002/adfm.202305965
44. Mahmoud NN, Aqabani H, Hikmat S, Abu-Dahab R. Colloidal stability and cytotoxicity of polydopamine-conjugated gold nanorods against prostate cancer cell lines. *Molecules*. 2021;26(5):1299. doi:10.3390/molecules26051299
45. Yang X, Li M, Liang J, Hou X, He X, Wang K. NIR-controlled treatment of multidrug-resistant tumor cells by mesoporous silica capsules containing gold nanorods and doxorubicin. *ACS Appl Mater Interfaces*. 2021;13(13):14894–14910. doi:10.1021/acsami.0c23073
46. Dash P, Thirumurugan S, Tseng C-L, et al. Synthesis of methotrexate-loaded dumbbell-shaped titanium dioxide/gold nanorods coated with mesoporous silica and decorated with upconversion nanoparticles for near-infrared-driven trimodal cancer treatment. *ACS Appl Mater Interfaces*. 2023;15(28):33335–33347. doi:10.1021/acsami.3c04300
47. Gulati S, Ansari N, Moriya Y, et al. Nanobiopolymers in cancer therapeutics: advancing targeted drug delivery through sustainable and controlled release mechanisms. *J Mater Chem B*. 2024;12(46):11887–11915. doi:10.1039/D4TB00599F
48. Zhu S, Gao H, Li W, et al. Stimuli-responsive aptamer-drug conjugates for targeted drug delivery and controlled drug release. *Adv Healthcare Mater*. 2024;13(23):2401020. doi:10.1002/adhm.202401020
49. Kucharczyk K, Florczak A, Kaminska A, et al. MMPs-responsive silk spheres for controlled drug release within tumor microenvironment. *Int J Biol Macromol*. 2024;269:132016. doi:10.1016/j.ijbiomac.2024.132016
50. Prince Y, Hiremath N, Vankayala R. Near-infrared light activatable niosomes loaded with indocyanine green and plasmonic gold nanorods for theranostic applications. *Biomater Sci*. 2023;11(24):7759–7767. doi:10.1039/D3BM01187A

International Journal of Nanomedicine

Publish your work in this journal

The International Journal of Nanomedicine is an international, peer-reviewed journal focusing on the application of nanotechnology in diagnostics, therapeutics, and drug delivery systems throughout the biomedical field. This journal is indexed on PubMed Central, MedLine, CAS, SciSearch®, Current Contents®/Clinical Medicine, Journal Citation Reports/Science Edition, EMBase, Scopus and the Elsevier Bibliographic databases. The manuscript management system is completely online and includes a very quick and fair peer-review system, which is all easy to use. Visit <http://www.dovepress.com/testimonials.php> to read real quotes from published authors.

Submit your manuscript here: <https://www.dovepress.com/international-journal-of-nanomedicine-journal>

Dovepress
Taylor & Francis Group